J. metamorphic Geol., 2004, **22,** 811–824 doi:10.1111/j.1525-1314.2004.00552.x

An analysis of uncertainty in non-equilibrium and equilibrium geothermobarometry

J. R. ASHWORTH[1,*], V. S. SHEPLEV[2,†], V. V. KHLESTOV[2] AND V. A. ANANYEV[2]
[1]*School of Geography, Earth and Environmental Sciences, University of Birmingham, Edgbaston, Birmingham B15 2TT, UK (ashworjr@geesmail.bham.ac.uk)*
[2]*United Institute of Geology, Geophysics and Mineralogy, Siberian Branch of Russian Academy of Science, Koptyug Pr. 3, Novosibirsk 630090, Russia*

ABSTRACT In statistically optimised *P–T* estimation, the contributions to overall uncertainty from different sources are represented by ellipses. One source, for a diffusion-controlled reaction at non-equilibrium, is diffusion modelling of the reaction texture. This modelling is used to estimate ratios, Q, between free-energy differences, ΔG, of reactions among mineral end-members, to replace the equilibrium condition $\Delta G = 0$. The associated uncertainty is compared with those already inherent in the equilibrium case (from end-member data, activity models and mineral compositions). A compact matrix formulation is introduced for activity coefficients, and their partial derivatives governing error propagation. The non-equilibrium example studied is a corona reaction with the assemblage Grt–Opx–Cpx–Pl–Qtz. Two garnet compositions are used, from opposite sides of the corona. In one of them, affected by post-reaction Fe, Mg exchange with pyroxene, the problem of reconstructing the original composition is overcome by direct use of ratios between chemical-potential differences, given by the diffusion modelling. The number of geothermobarometers in the optimisation is limited by near-degeneracies. Their weightings are affected by strong correlations among Q ratios. Uncertainty from diffusion modelling is not large in comparison with other sources. Overall precision is limited mainly by uncertainties in activity models. Hypothetical equilibrium *P–T* are also estimated for both garnet compositions. By this approach, departure from equilibrium can be measured, with statistical uncertainties. For the example, the result for difference from equilibrium pressure is 1.2 ± 0.7 kbar.

Key words: corona; diffusion; geothermobarometry; non-equilibrium; uncertainties.

INTRODUCTION

A line in *P–T* space, defined by combining mineral compositions with experimental calibration, can be termed a geothermobarometer (GTB). Finding a *P–T* point from GTBs usually embodies the basic assumption or approximation of equilibrium at that point, which is a possible source of systematic error that cannot readily be quantified. Other uncertainties, from the experimental work and mineral analyses, are treatable statistically. For three GTBs, Hodges & McKenna (1987) calculated uncertainty bands in *P–T* space arising from experimental calibration alone. These uncertainties are much larger than those attributed to analytical errors. In general, there are two experimental sources of uncertainty: *P–T* calibration of pure end-member equilibria, and estimation of activity in solid solution. For the Grt–Ky–Pl–Qtz geobarometer, Kohn & Spear (1991) considered both separately, finding that each exceeded the uncertainties from analytical method and natural compositional heterogeneity.

An important advance has been the compilation of thermodynamic data sets for mineral end-members. These are obtained by combining large amounts of experimental data (Holland & Powell, 1985; Berman, 1988). From one of these data sets together with mineral analyses and activity models, an optimised *P–T* point estimate is obtained, surrounded by an uncertainty ellipse (Powell & Holland, 1994). The method used to define this ellipse has also been applied to uncertainties in phase-diagram drawing (Powell *et al.*, 1998).

A further development is non-equilibrium geothermobarometry. For example, in the case of a corona that grew under diffusion control, diffusion modelling gives ratios of ΔG, for use in GTBs instead of $\Delta G = 0$. For the corona style shown schematically in Fig. 1, that method was demonstrated by Ashworth *et al.* (2001). The use of ratios eliminates absolute diffusion coefficients, whose values would be very uncertain. The method of ratios is likely to be applicable to other kinds of reaction texture. In this paper, non-equilibrium geothermobarometry is examined statistically, using the example corona of Fig. 1, with the aims of

**Present address:* J. R. Ashworth, 80 Selly Wick Drive, Birmingham B29 7JH, UK.
†Deceased.

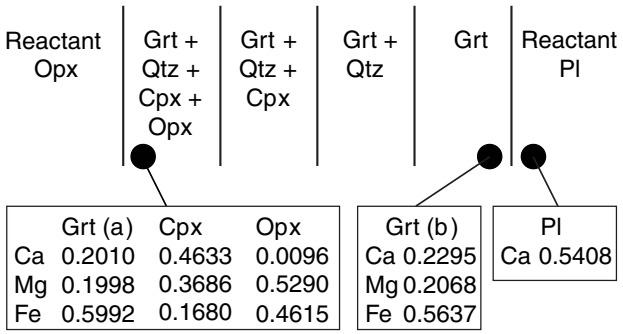

Fig. 1. Diagram of the layers in the corona described in detail by Ashworth *et al.* (1998), in a metabasic granulite from the Yenisey Ridge, Siberia. Layer thicknesses are not to scale. The Grt + Qtz + Cpx + Opx layer is slightly modified from reactant orthopyroxene (which includes exsolved grains of clinopyroxene). Generalised locations of mineral analyses are labelled with compositions. These are statistical averages except that Mg and Fe contents of garnet (a) have been reconstructed to correct for retrograde diffusive exchange with the pyroxenes (Ashworth *et al.*, 1998), which are volumetrically predominant and are assumed not to have changed noticeably.

comparing uncertainties from diffusion modelling with those from other sources and assessing the precision of the non-equilibrium$P$–T estimate. The diffusion-modelling uncertainties are shown to be small enough that the method is justified. The non-equilibrium result is compared with hypothetical equilibrium pressures and temperatures defined by the same mineral analyses. The difference between non-equilibrium and equilibrium is treated using the statistics of P–T differences following Worley & Powell (2000). Refinements of theory, and the simple example, enable some comments to be made on geothermobarometry more generally.

NON-EQUILIBRIUM GEOTHERMOBAROMETRY

For two reactions A and B among end-members in the minerals, diffusion modelling can estimate the Q ratio defined by

$$Q = \frac{\Delta G_{\mathrm{A}}}{\Delta G_{\mathrm{B}}} \qquad (1)$$

Q is found from relative differences in chemical potential $\delta\mu_i/\delta\mu_j$ for components i, j, measured between two locations in a reaction texture. These differences drive diffusion during reaction. Assumptions or approximations are of three kinds.

(**1**) The reaction was diffusion-controlled, with local equilibrium maintained at every point. Non-zero ΔG arises from minerals not being in contact, and also from spatial variation in mineral compositions.

(**2**) Diffusion is described by Onsager coefficients L_{ii}, by which the diffusive flux of component i is proportional to gradient $-(\mathrm{d}\mu_i/\mathrm{d}z)$. Ratios among coefficients are taken to be constants. Another constraint is the Gibbs–Duhem equation; in the presence of phase k,

$$\sum_i n_{ik}\left(\frac{\mathrm{d}\mu_i}{\mathrm{d}z}\right) = 0 \qquad (2)$$

where n_{ik} is the number of moles of i in one mole of k. Cross-coefficients L_{ij}, by which $\mathrm{d}\mu_j/\mathrm{d}z$ would influence the flux of i, are neglected. Ratios, usually L_i/L_{Si}, are inputs for the modelling. The components are oxides, so Si stands for SiO_2, Al for $AlO_{3/2}$, etc. The real diffusion process must be more complex. However, an oxide component (MgO) has been identified as controlling corona growth in a simple experimental system (Milke *et al.*, 2001). In natural coronas, as in the experiments, diffusion occurs mainly along grain boundaries. In the natural case, different kinds of boundary exist (between different minerals); diffusion cannot everywhere be the same. Nevertheless, the modelling successfully reproduces in detail the observed layered structures (e.g. Ashworth & Sheplev, 1997).

(**3**) The stoichiometric coefficients in the overall reaction, including any metasomatic fluxes (across the boundaries of the modelled domain), are constrained by quantitative petrography and mineral compositions. Unless there is evidence that the reaction changed with time, it is assumed to have remained constant. Thus the mineral compositions give a single P–T estimate, as if the original (corona-free) rock experienced a sudden change of P and/or T then remained at one P–T point while the corona grew. This approximation is comparable with that of equilibrium at fixed P–T in conventional geothermobarometry. The non-equilibrium estimate is regarded as an effective or averaged P and T of reaction.

The P–T line of a non-equilibrium GTB is defined by

$$\Delta G_{\mathrm{A}} - Q\Delta G_{\mathrm{B}} = 0.$$

A range of L-ratios will give acceptable models (satisfactorily matching petrographic data), leading to ranges in Q estimates. This source of uncertainty is additional to those in equilibrium geothermobarometry. Because differences ($\delta\mu$,ΔG) are modelled, the natural approach to least-squares optimisation is to use weighted GTBs (Powell & Holland, 1988, 1994), rather than weighted free energies of individual end-members (Gordon, 1992).

THE YENISEY EXAMPLE

The Yenisey corona schematically shown in Fig. 1 grew by an overall reaction that is essentially

$$\mathrm{Opx} + \mathrm{Pl} \rightarrow \mathrm{Grt} + \mathrm{Cpx} + \mathrm{Qtz}.$$

Overall stoichiometry is constrained by the lack of other major minerals to act as sources or sinks for components. Exchange of Ca, Fe and Mg across the boundary with reactant pyroxene is allowed. As the corona contains very little Na, albite component was retained within reactant plagioclase. Thus the reaction is well described within the five-component system

Table 1. A set of independent reactions, and the set of GTBs used, for the Yenisey example.

Reactions:
1. 3 an + 3 di = 1 py + 2 gr + 3 q
2. 3 an + 3 en = 2 py + 1 gr + 3 q
3. 3 fs + 2 py = 3 en + 2 alm
4. 3 hed + 1 py = 3 di + 1 alm

Geothermobarometers: Numbers refer to the reactions above.
Letters (a, b) refer to use of Grt (a) or Grt (b) of Fig. 1.
2b/1a: $Q_{2b/1a} = \Delta G_{2b}/\Delta G_{1a} \approx 0.188$
4b/2a: $Q_{4b/2a} = \Delta G_{4b}/\Delta G_{2a} \approx 0.421$
3a: $Q = 0$ (equilibrium)
4a: $Q = 0$ (equilibrium)

CFMAS. Nine end-members are useful in GTBs (alm, py, gr, en, fs, di, hed, an, q; notation of Holland & Powell, 1998). The number of independent end-member reactions (Powell & Holland, 1988, Appendix B) is thus $9 - 5 = 4$. These correspond to GTBs for use at equilibrium (used for hypothetical equilibrium below). The chosen set is numbered 1–4 in Table 1. The first two are well-known geobarometric reactions, while 3 and 4 are familiar as Fe–Mg exchange geothermometers (e.g. Spear, 1993, p. 534). All the minerals have well-developed activity models (Appendix A contains matrix formulations for ease of computation).

Garnet is zoned across the corona. Compositions near both edges, (a) and (b) in Fig. 1, are used in the non-equilibrium GTBs. For each reaction, ΔG can be estimated using either garnet composition (a) or (b). Garnet (a) coexists with pyroxene at assumed equilibrium, but (b) does not. The chosen set of four GTBs (Table 1) includes two with Q ratios between (b) and (a) reactions; values of Q in Table 1 are means from the diffusion-modelling study summarised below. The other two are equilibrium GTBs with garnet (a): the geothermometers for garnet–orthopyroxene (3a) and garnet–clinopyroxene (4a). It might be thought that, with additional information (second garnet composition) relative to the equilibrium case, the number of GTBs in the non-equilibrium set would exceed four. Appendix B (section on near-degeneracy) explains the restriction to four and the reason for including two equilibrium GTBs. A complicating feature of the example is that Mg and Fe contents of garnet (a) have been altered by retrograde exchange (Ashworth *et al.*, 1998, p. 241). In Fig. 1, the original composition has been reconstructed approximately, by using ratios of chemical-potential differences from the diffusion modelling. In the geothermobarometry below, the uncertainties because of reconstruction are minimised by making direct use of these modelling results.

SOURCES OF UNCERTAINTY IN GENERAL

Uncertainties come from four sources, represented by square blocks of the matrix **V** in Fig. 2. The uncertainties arising in the diffusion modelling (block labelled Q in Fig. 2) are compared with the other three blocks, for thermodynamic data, activity models and mineral compositions, as identified below:

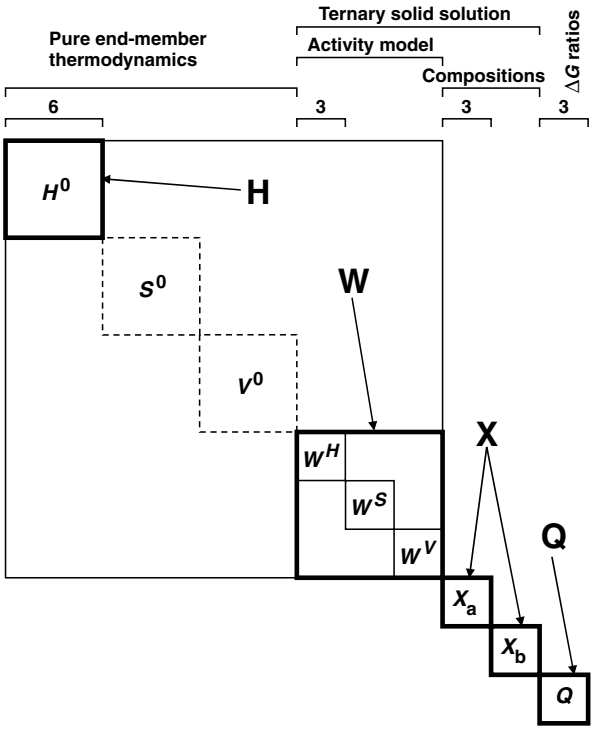

Fig. 2. Block structure of the matrix **V** comprising variances and covariances of quantities used in P–T estimation. For clarity, this is drawn for a simpler system than that in the Yenisey example, with three components, and six mineral end-members (a ternary solid solution and three minerals of fixed composition). The solid solution has a symmetrical activity model (Margules parameters $W_i, i = 1,2,3$, and $W_i = W_i^H - TW_i^S + PW_i^V$ following Thompson, 1967), with its composition measured at two locations (a, b). In this hypothetical system, three non-equilibrium GTBs are used [three non-zero ratios Q in Eq. (1)]. Within the heavily outlined squares, covariances should be non-zero. The labels H, W, X and Q identify the four blocks, respectively for end-member thermodynamic data, activity modelling, mineral compositions and diffusion-modelling results. The H block contains the enthalpy uncertainties of Holland & Powell (1998); the diagram also admits possible uncertainties in S^0 and V^0. Within the large, lightly outlined square containing both H and W, covariances exist in principle and could be entered if known.

(**1**) end-member thermodynamic data, labelled H because the approach of Powell & Holland (1985) assigns all uncertainty to enthalpy, H^0. The block would be larger if uncertainty was distributed among more quantities (S^0 and V^0 are suggested in Fig. 2).
(**2**) activity models, labelled W for Margules parameter.
(**3**) mineral compositions, labelled X for mole fraction. Entering mole fractions (i.e. recalculated rather than raw analyses) may improve precision, because some outlying analyses can be rejected as having poor stoichiometry.

Uncertainties in the estimate of P or T (P_{est} or T_{est}) from a GTB are calculated from matrix **V** using vector $\mathbf{J}_P$ or $\mathbf{J}_T$, respectively containing $\partial P_{est}/\partial y_j$ and $\partial T_{est}/\partial y_j$ for quantities y_j in all blocks (Powell, 1985). If the

blocks are uncorrelated (covariances are zero outside the heavily outlined squares in Fig. 2), the calculation can be decomposed into four parts. Writing σ^2 for $\sigma^2_{P_{est}}$ or $\sigma^2_{T_{est}}$, and $\mathbf{J}$ for $\mathbf{J}_P$ or $\mathbf{J}_T$,

$$\sigma^2 = \mathbf{J}_H\mathbf{V}_H\mathbf{J}_H^{\mathrm{T}} + \mathbf{J}_W\mathbf{V}_W\mathbf{J}_W^{\mathrm{T}} + \mathbf{J}_X\mathbf{V}_X\mathbf{J}_X^{\mathrm{T}} + \mathbf{J}_Q\mathbf{V}_Q\mathbf{J}_Q^{\mathrm{T}}. \tag{3}$$

This is like Eq. (13) of Worley & Powell (2000), with the addition of the Q term.

Activity models generally depend on the end-member data (e.g. Mukhopadhyay *et al.*, 1997), theoretically linking the H and W blocks. It seems possible that future work will produce a block consolidating these, with full array of covariances (large square in Fig. 2). In principle, the outcomes of diffusion modelling (Q block) depend on the mineral compositions X, but the effect of varying X is small. In the example studied, acceptable modelling involves ranges of L-ratios that introduce uncertainties in Q several orders of magnitude larger than those arising from uncertainties in mineral compositions. The diffusive fluxes are governed by large compositional differences between minerals; e.g. large fluxes of Fe and Mg to the plagioclase boundary in Fig. 1 are required for garnet to grow there. Slight changes in mineral compositions have negligible effect on fluxes. This should be true of diffusion-controlled metamorphic reactions in general. Therefore, the X and Q blocks can be treated as uncorrelated.

Correlations are important within the H block (Powell & Holland, 1985), and presumably within W, though rarely tabulated for that block. In the X block, mole fractions sum to 1 and are certainly correlated; each row or column of their variance–covariance matrix must sum to zero [Chayes, 1971, Eq. (4.2)]. In a ternary mineral (garnet in the example), the covariances depend only on the variances:

$$\mathrm{Cov}(X_1, X_2) = \frac{1}{2}[\sigma^2_{X_3} - (\sigma^2_{X_1} + \sigma^2_{X_2})]. \tag{4}$$

SOURCES OF UNCERTAINTY IN THE YENISEY EXAMPLE

For end-member thermodynamics, the data set of Holland & Powell (1998) is adopted, with its variances and covariances. For Margules parameters, except in garnet, the general estimate of Worley & Powell (2000, p. 94) is used for approximate uncertainties.

Garnet activity model

Mukhopadhyay *et al.* (1997) made a considerable advance by publishing uncertainties along with Margules parameters. Unfortunately, these are variances only; covariances are not available. Use of the variances alone in this paper is defensible empirically, as follows. Two other activity studies (Berman & Aranovich, 1996; Ganguly *et al.*, 1996) are comparable with that of Mukhopadhyay *et al.* (1997). Strict treatment of the Mukhopadhyay uncertainties (with covariances) might not embrace the other two models within the uncertainty bands (Holdaway, 2000, Fig. 1). However, use of the uncorrelated variances gives GTB bands (Fig. 3) containing the GTB lines from the other models, though for GTB 2b/1a these lines are relatively close to the band boundaries. Therefore, the approach gives a fair, perhaps slightly cautious assessment of the precision for currently used garnet activity models.

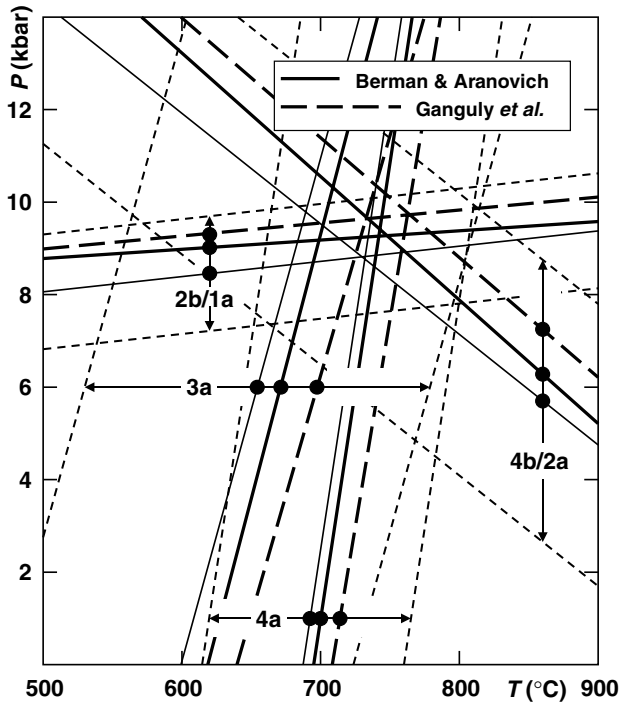

Fig. 3. P–T diagram showing uncertainties, of individual GTBs, calculated from uncertainties in garnet activity model alone. The GTBs 2b/1a, 4b/2a, 3a and 4a are defined in Table 1. For each of these, light dashed lines define an uncertainty band ($\pm 2\sigma$) about the central light solid line; the central line is calculated using Margules parameters of Mukhopadhyay *et al.* (1997), and the uncertainty band is calculated from their variances. The bands are linearised using the central approximation of Appendix B. In each case, heavy lines calculated from the alternative activity models (Berman & Aranovich, 1996; Ganguly *et al.*, 1996) lie within the uncertainty bands from Mukhopadhyay *et al.* (1997).

Mineral compositions

The mineral compositions used (Fig. 1) are statistical means, and thus differ slightly from the representative analyses used previously (Ashworth *et al.*, 1998, 2001). Table 2 gives 2σ uncertainties and correlations. Because the sample size N is small, Student's t is used in estimating 2σ (Davis, 2002, p. 72). For the 95% confidence interval,

$$2\sigma = t_{0.05,N-1}\left(\frac{S}{\sqrt{N}}\right) \tag{5}$$

where S is the sample standard deviation.

Table 2. Mineral composition statistics for the Yenisey example.

	2σ (×100)	Correlation coefficients		
Garnet (a) (reconstructed)				
X_{Ca}	0.60	1	−0.300	−0.300
X_{Mg}	1.00		1	−0.820
X_{Fe}	1.00			1
Garnet (b) ($n = 5$)				
X_{Ca}	0.93	1	−0.793	−0.289
X_{Mg}	0.95		1	−0.354
X_{Fe}	0.61			1
Opx ($n = 9$), X_{Fe}	1.09			
Cpx ($n = 9$), X_{Fe}	0.90			
Pl ($n = 4$), X_{Ca}	1.07			

In Opx, Ca is neglected : $X_{Fe} = Fe/(Mg + Fe)$. In Cpx, $X_{Fe} = Fe/(Ca + Mg + Fe)$.

Reconstruction of X_{Mg} and X_{Fe} in garnet (a) (Fig. 1) uses mean values of $X_{Ca,a}$ and the following ratios, estimated by the diffusion modelling:

$$\zeta_{py} = \frac{\delta\mu_{py}}{\delta\mu_{gr}} \quad \text{and} \quad \zeta_{alm} = \frac{\delta\mu_{alm}}{\delta\mu_{gr}}$$

where $\delta\mu_i$ is a chemical-potential difference between locations (a) and (b):

$$\delta\mu_i = \mu_{ia} - \mu_{ib}. \tag{6}$$

Reconstruction also uses the activity model. Rather than writing complicated relationships among X, W and Q blocks, generous 2σ estimates are given to reconstructed X_{Mg} and X_{Fe} (Table 2, with covariances from Eq. (4)), but their influence is minimised by using ζ_i directly in the geothermobarometry. This transfers some uncertainty to the modelling. For a reaction with garnet (a), ΔG is estimated by

$$\Delta G_a = \Delta G_b + (\mu_{gr,a} - \mu_{gr,b})\Delta\zeta$$

where $\Delta\zeta$ includes a term for grossular with $\zeta_{gr} = 1$. The reconstructed quantities $X_{Mg,a}$ and $X_{Fe,a}$ enter only into calculating the activity coefficient of grossular.

Diffusion modelling

The Q block (unlike that in Fig. 2) now represents two ζ variables in addition to Q ratios, but only two of the latter are non-zero: the outputs from diffusion modelling used in geothermobarometry are $Q_{2b/1a}$, $Q_{4b/2a}$, ζ_{py} and ζ_{alm}. The variables used as inputs to the modelling are diffusion-coefficient ratios L_{Ca}/L_{Si}, L_{Fe}/L_{Si}, L_{Mg}/L_{Si}, L_{Al}/L_{Si}, and stoichiometric coefficients in the overall reaction. The restrictions on metasomatism (ab, an exchange with plagioclase; Fe, Ca, Mg exchange with reactant pyroxene) amount to closure equations for Al and Si. Therefore the modelling is not mathematically overdetermined (Ashworth & Birdi, 1990, Table 2). This precludes use of the least-squares method, developed by Foster (1981) for reaction textures and applied specifically to coronas by Markl *et al.* (1998). Instead, sampling over a range of inputs gives a range of models. A model is rejected unless consistent with petrographic data, namely that the observed layer sequence (Fig. 1) must be reproduced, with garnet and quartz contents of the Grt + Cpx + Qtz layer in the respective ranges 6.5–13.5 and 16–27 volume percent. To be accepted, a model must also produce ζ_i consistent with the observed compositional difference across the monomineralic garnet layer (where retrograde modification should be negligible).

Three of the input variables are not well constrained, but fortunately have relatively little influence on the results. One is L_{Al}/L_{Si} which, however, is very unlikely to differ from unity by more than an order of magnitude, as the other L_i/L_{Si} are found to be within that range. The other two poorly constrained inputs are stoichiometric coefficients in the overall reaction. The boundary between reactant pyroxene and the slightly modified layer in Fig. 1 is difficult to locate precisely; this leaves ambiguity over the partitioning of Ca, Mg, Fe between pyroxene in the growing corona and metasomatic diffusive exchange across the boundary. The adjustable coefficients are ν_{Cpx} and ν_{Opx} for corona pyroxenes. Variation of these by $\pm 50\%$ would be consistent with the petrographic data. To accommodate this uncertainty and that in L_{Al}/L_{Si}, sampling was done at the seven nodes in Fig. 4a. Within each node, grid sampling was used for the other three inputs (Fig. 4b).

Relative to the central node alone, the other six extend the range of results by less than a factor of 2 (Fig. 5). Table 3 summarises the statistics. Here, 2σ is simply twice the standard deviation in the sample, not divided by $\sqrt{N}$ as in Eq. (5), which is because the variation is not simply random perturbation of a central value. If the sample size N was increased (as could easily be done, by decreasing the grid interval of Fig. 4b), the uncertainties for these variables, exemplified in Fig. 5, would remain essentially the same.

Correlations are found among the modelling outputs (Table 3, Fig. 5). In general, some covariance may be induced mathematically by using ratios (Chayes, 1971). However, the two very strong correlations (coefficients < -0.98, Table 3) are meaningful. The two ζ_i are almost exactly interdependent because garnet is only slightly zoned. From the Gibbs–Duhem equation [Eq. (2)], for Ca–Mg–Fe garnet of fixed composition,

$$X_{Ca}\frac{d\mu_{gr}}{dz} + X_{Mg}\frac{d\mu_{py}}{dz} + X_{Fe}\frac{d\mu_{alm}}{dz} = 0.$$

Hence, with nearly constant garnet composition,

$$X_{Ca} + X_{Mg}\zeta_{py} + X_{Fe}\zeta_{alm} \approx 0.$$

The strong correlation between $Q_{2b/1a}$ and $Q_{4b/2a}$ (Table 3) implies an approximate linear relationship among the model analogues of free-energy difference, $\Delta G^*_{4b}, \Delta G^*_{2b}$, ΔG^*_{2a} and ΔG^*_{1a}. The last two are exactly equal; in combination, they represent an equilibrium between garnet (a) and coexisting pyroxene

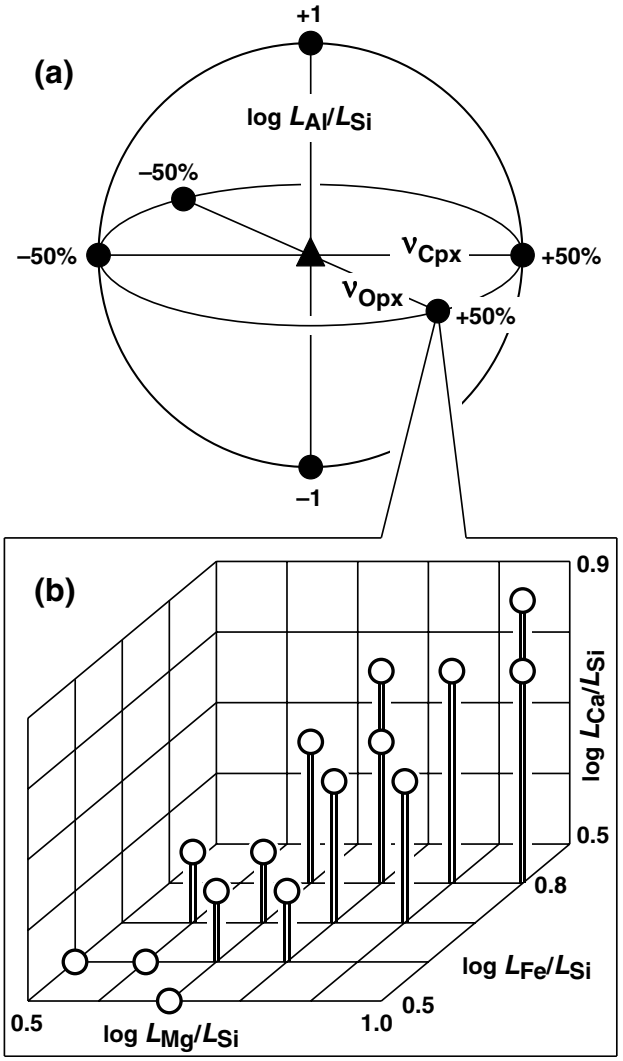

Fig. 4. Sampling scheme used in diffusion modelling. (a) Sphere representing the seven nodes used for the poorly constrained variables: one central node (filled triangle), and an outlying pair for each variable. (b) Sketch of a three-dimensional grid to show sampling with a $\log_{10}$ interval of 0.1 for the other three variables. Shown are the actual 15 points found to give acceptable models at the node for ν_{Opx} + 50%.

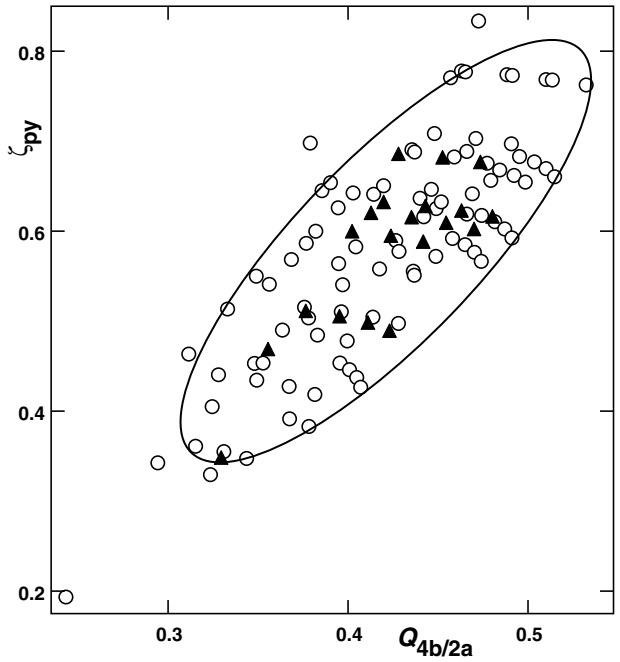

Fig. 5. Scatter diagram for outputs from diffusion modelling. Each point represents the value of ζ_{py} and $Q_{4b/2a}$ at one of the 110 sample points giving acceptable fits to the quantitative petrography and garnet zoning data for the observed corona. Filled triangles are from points at the central node in Fig. 4, and open circles are from other nodes. Also shown is the 2σ uncertainty ellipse. Because of strong correlations (Table 3) between $Q_{4b/2a}$ and $Q_{2b/1a}$ and between ζ_{py} and ζ_{alm}, a plot of either of these pairs would be an almost linear array, and plots of other pairings would approximately mirror that shown here.

Table 3. Summary of diffusion modelling results.

	Mean	2σ	Correlation coefficients			
$Q_{2b/1a} = \Delta G^*_{2b}/\Delta G^*_{1a}$	0.188	0.178	1	−0.987	−0.707	0.714
$Q_{4b/2a} = \Delta G^*_{4b}/\Delta G^*_{2a}$	0.421	0.113		1	0.809	−0.815
$\zeta_{py} = \delta\mu^*_{py}/\delta\mu^*_{gr}$	0.578	0.236			1	−0.994
$\zeta_{alm} = \delta\mu^*_{alm}/\delta\mu^*_{gr}$	−0.542	0.079				1

*Indicates the model quantity proportional to the thermodynamic one (Ashworth & Sheplev, 1997); $\delta\mu$ is defined by Eq. (6).

$$(1a - 2a): 3di + 1py(a) = 3en + 1gr(a).$$

The relationship found among the other variables is

$$\Delta G^*_{2a} - \Delta G^*_{2b} - 2\Delta G^*_{4b} \approx 0. \quad (7)$$

This is not an (approximate) equilibrium, because it involves garnet of both compositions (a, b). It arises from the strong observational constraints on the modelling, and is related to the narrow range of ζ_i permitted by the data. Each ΔG^* is a combination of differences $\delta\mu^*$, analogous to Eq. (6), for oxide components i. These components at location (b) of Fig. 1 make up plagioclase and garnet (b), and at location (a) pyroxenes, quartz and garnet (a). In these terms, the left-hand side of Eq. (7) is

$$3\delta\mu^*_{CaO} + 6\delta\mu^*_{FeO} + 3\delta\mu^*_{Al_2O_3} + 9\delta\mu^*_{SiO_2}$$

which equals $\delta\mu^*_{gr} + 2\delta\mu^*_{alm}$, so that Eq. (7) would be exact if ζ_{alm} was exactly −0.5.

CONTRIBUTIONS OF SOURCES TO OPTIMISED UNCERTAINTIES

A theoretical basis is required for defining a separate uncertainty ellipse for each block (Fig. 6). The weighted averages P_{ave}, T_{ave} give lines which intersect at the optimised point P_{opt}, T_{opt}. Uncertainty bands for P_{ave}, T_{ave} could be drawn using $\mathbf{J}_{P_{ave}}$ and $\mathbf{J}_{T_{ave}}$ [Appendix B, Eq. (B1)] and can be split as in Eq. (3) to give sub-

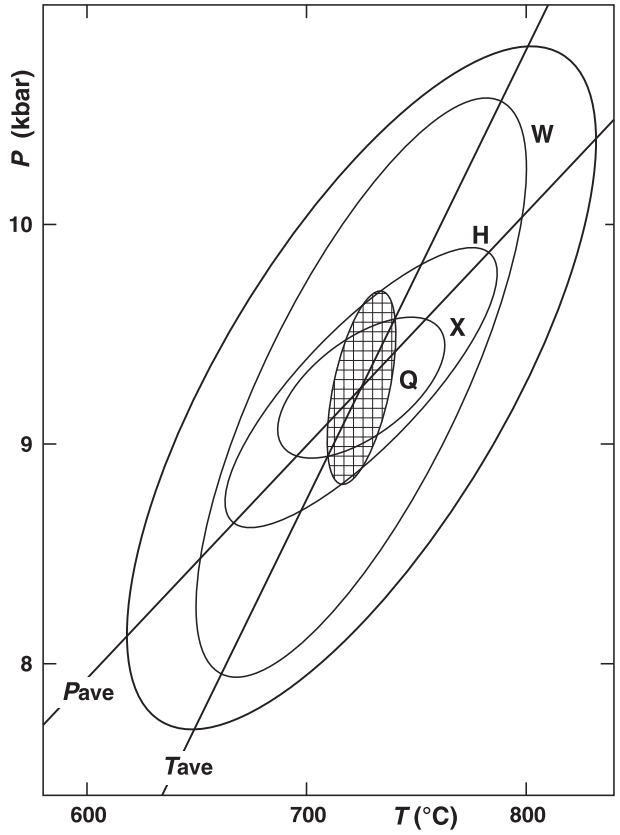

Fig. 6. P–T diagram showing uncertainty ellipses (2σ) for the Yenisey non-equilibrium example. The labelling corresponds to the blocks defined in Fig. 2. Inside the overall ellipse are those for the four blocks W, H, X and Q. The Q ellipse, which is the special feature associated with non-equilibrium, is picked out by cross-hatch ornament. The lines for P_{ave} and T_{ave} intersect at $P_{opt} = 9.26$ kbar, $T_{opt} = 725$ °C.

bands defined by $\sigma_{P_{ave},\lambda}$ and $\sigma_{T_{ave},\lambda}$ ($\lambda = H, W, X, Q$). Each band is tangent to the ellipse for λ uncertainty in P_{opt}, T_{opt}, drawn by Eq. (4) of Powell & Holland (1988) with parameters $\sigma_{P_{opt},\lambda}$,$\sigma_{T_{opt},\lambda}$ and ρ_λ, found from splitting $\mathbf{J}_{P_{opt}}$ and $\mathbf{J}_{T_{opt}}$ of Appendix B, Eq. (B2a,b). The block variances $\sigma^2_{P_{opt},\lambda}$ sum to the overall variance $\sigma^2_{P_{opt}}$; likewise $\sigma^2_{T_{opt},\lambda}$, and $\mathrm{Cov}(P_{opt}, T_{opt})_\lambda$ given by

$$\mathrm{Cov}(P_{opt}, T_{opt})_\lambda = \mathbf{J}_{P_{opt},\lambda}\mathbf{V}_\lambda\mathbf{J}^{\mathrm{T}}_{T_{opt},\lambda}.$$

Whereas the overall $\sigma_{P_{opt}}$ and $\sigma_{T_{opt}}$ cannot be smaller than $\sigma_{P_{ave}}$ and $\sigma_{T_{ave}}$, respectively, $\sigma_{P_{opt},\lambda}$ and $\sigma_{T_{opt},\lambda}$ may be less than $\sigma_{P_{ave},\lambda}$ and $\sigma_{T_{ave},\lambda}$, particularly if ρ_λ is opposed in sign to overall ρ (e.g. for W of orthopyroxene).

The above method gives valid representations of the uncertainties from different sources, under the condition that the weightings of GTBs used throughout are those defined by the overall uncertainties. An alternative approach would be to use each block in isolation, to find separate weightings and ellipses. However, the variances and covariances would not then sum to the correct overall values. Also, in the example, the strong correlations among Q (Table 3) prevent definition of weightings using the Q block alone (as explained more fully near the end of Appendix B).

RESULTS

For the Yenisey example, the determined P–T are 9.3 ± 1.6 kbar and 725 ± 106 °C. The result satisfies the goodness-of-fit test for mutual consistency of GTBs (Powell & Holland, 1988, p. 196; Powell & Holland, 1994, p. 127) with $\sigma_{fit} = 0.71$, less than the critical value of 1.61 for 95% confidence. The largest source of uncertainty is activity modelling (W, Fig. 6), as is often the case (Worley & Powell, 2000, p. 92). Uncertainties because of non-equilibrium produce the Q ellipse, which is not large in comparison with those for the other three blocks. This example shows that non-equilibrium need not greatly reduce the precision of P–T estimation relative to an equilibrium case.

The strong correlation between Q ratios (Table 3) has its main effect in the weightings. It is the principal reason for negative weightings, and those >1 in magnitude, shown in Table 4. A more closely grouped set of weightings could be obtained by choosing a different set of GTBs, but this seems unnecessary as the calculated uncertainties are stable (Appendix B).

Table 4 also breaks down the results into sub-blocks for individual minerals, where these are separable as being uncorrelated (X block and, in the current state of knowledge, W). Simple compositions and activity models lead to perfect correlation ($\rho_\lambda = \pm 1$) where there is only one variable y ($=W$ or X). The coefficient is -1 if $\partial P_{opt}/\partial y$ and $\partial T_{opt}/\partial y$ have opposite signs.

Table 4. Calculated weightings, standard deviations and correlation coefficients for the Yenisey non-equilibrium example.

	2b/1a	4b/2a	3a	4a	
Weightings in					
P_{ave}	2.116	−1.039	0.077	−0.154	
T_{ave}	0.474	2.062	0.424	−1.961	
	$\sigma_{Pave,\lambda}$ (kbar)	$\sigma_{Tave,\lambda}$ (°C)	$\sigma_{Popt,\lambda}$ (kbar)	$\sigma_{Topt,\lambda}$ (°C)	ρ_λ
Uncertainties following optimisation when λ=					
H	0.197	20.1	0.321	30.7	0.814
W Grt	0.278	16.0	0.548	34.2	0.891
W Opx	0.327	17.3	0.298	2.8	−0.9999
W Cpx	0.015	7.0	0.187	16.2	1
W Pl	0.087	4.0	0.093	0.6	1
All W	0.438	24.9	0.657	37.9	0.760
X Grt(a)	0.116	8.8	0.047	6.5	−1
X Grt(b)	0.117	10.5	0.100	12.0	0.495
X Opx	0.003	0.1	0.008	0.5	1
X Cpx	0.023	7.5	0.116	13.2	1
X Pl	0.005	0.2	0.005	0.03	1
All X	0.167	15.6	0.161	19.0	0.598
Q	0.188	9.2	0.220	7.8	0.545
	σ_{Pave}	σ_{Tave}	σ_{Popt}	σ_{Topt}	ρ
Overall	0.542	36.8	0.781	53.0	0.720

The uncertainties for orthopyroxene are strongly reduced by symmetry effects. The Mg and Fe end-members are about equally represented in both (i) contributions to P_{ave} or T_{ave}, and (ii) the mineral composition. Effect (i) can be stated in terms of $\partial P_{ave}/\partial \mu_i$ and $\partial T_{ave}/\partial \mu_i$ (see Appendix C of Supplementary Material), thus:

$$\frac{\partial P_{ave}}{\partial \mu_{en}} \approx \frac{\partial P_{ave}}{\partial \mu_{fs}} \quad \text{and} \quad \frac{\partial T_{ave}}{\partial \mu_{en}} \approx \frac{\partial T_{ave}}{\partial \mu_{fs}} \qquad (8)$$

(Table 5). It is perhaps surprising that $\partial T_{ave}/\partial \mu_{en}$ and $\partial T_{ave}/\partial \mu_{fs}$ are similar, or even that they have the same sign, as the two end-members are on opposite sides of the reaction for the simple garnet–orthopyroxene geothermometer. The similarity arises, in the weighted averaging, from the two end-members being similarly affected by uncertainties. It can be described as follows. The set of GTBs could be recast so that only one involved enstatite and only one ferrosilite, with equal coefficients $v_A - Qv_B$. Then, from Eq. (C1) (see Appendix C of Supplementary Material), if these GTBs had similar entropy terms s, they would also have similar weightings in T_{ave}; also, with similar v, they would have similar weightings in P_{ave}.

Effect (ii), the nearly central composition in the symmetrical solid solution, has consequences outlined in Appendix C of Supplementary Material [Eq. (C7)]. With respect to the only X-block variable,

$$\frac{\partial \mu_{en}}{\partial X_{Fe}} \approx \frac{-\partial \mu_{fs}}{\partial X_{Fe}} \qquad (9)$$

(Table 5). The dependence of P_{ave} on the single variable is $\partial P_{ave}/\partial X_{Fe} = (\partial P_{ave}/\partial \mu_{en}\partial \mu_{en}/\partial X_{Fe}) + (\partial P_{ave}/\partial \mu_{fs}\partial \mu_{fs}/\partial X_{Fe})$.

Through near-equalities (8) and (9), the two terms nearly cancel here, and analogously in $\partial T_{ave}/\partial X_{Fe}$.

The nearly equal dependence of μ_{en} and μ_{fs} on each W (Table 5) makes this essentially a single-variable case, as if there was a single $\mu(=\mu_{en} + \mu_{fs})$. As $\partial P_{opt}/\partial \mu$ and $\partial T_{opt}/\partial \mu$ have opposed signs (Table 5), $\rho_W \approx -1$, $\sigma_{P_{opt},W} < \sigma_{P_{ave},W}$ and $\sigma_{T_{opt},W} < \sigma_{T_{ave},W}$ (Table 4).

For plagioclase, both X and W give very small uncertainties (Table 4), because the activity of anorthite is insensitive to both activity model and small changes in composition, near $X_{Ca} = 0.5$ at $T \approx 700$ °C (Holland & Powell, 1992). The limited importance of small errors in X for both plagioclase and orthopyroxene is fortunate in the present example, because these are the reactant minerals and are likely to have changed slightly in composition during reaction.

Garnet gives the largest W uncertainties in both P_{opt} and T_{opt}. Compositionally, garnet (a), with the use of ζ, is exactly a single-variable case with μ_{gr} as the only independent chemical potential. Opposed signs of $\partial P_{opt}/\partial \mu$ and $\partial T_{opt}/\partial \mu$ give correlation −1, hence $\sigma_{P_{opt},X} < \sigma_{P_{ave},X}$ and $\sigma_{T_{opt},X} < \sigma_{T_{ave},X}$ (Table 4). Further discussion of garnet is deferred to the simpler equilibrium case with no ζ.

Table 5. Calculated quantities for orthopyroxene in the Yenisey non-equilibrium example.

	i = en	fs
Partial derivatives of μ_i:		
$\partial \mu_i/\partial X_{Fe}$, kJ/mol	−33.5	38.4
$\partial \mu_i/\partial W_{enfs}$	0.067	0.076
$\partial \mu_i/\partial W_{fm}$ ($W_{fm} = W_{enfm} = W_{fsfm}$)	0.241	0.257
Partial derivatives with respect to μ_i:		
$\partial P_{ave}/\partial \mu_i$, kbar (kJ/mol)$^{-1}$	−0.330	−0.302
$\partial T_{ave}/\partial \mu_i$, °C (kJ/mol)$^{-1}$	18.1	15.4
$\partial P_{opt}/\partial \mu_i$, kbar (kJ/mol)$^{-1}$	−0.286	−0.288
$\partial T_{opt}/\partial \mu_i$, °C (kJ/mol)$^{-1}$	4.1	1.3

Hypothetical equilibria

Small uncertainties from non-equilibrium (Q, Fig. 6) do not imply comparably small departure from equilibrium during the reaction. This is demonstrated by estimating P and T for hypothetical equilibrium among the analysed minerals. Reactions 1–4 of Table 1 are used as equilibrium GTBs. With two garnet compositions (a, b), there are two hypothetical equilibria (Fig. 7), respectively using GTBs 1a–4a and 1b–4b in the notation of Table 1. Both satisfy the goodness-of-fit criterion, with σ_{fit} of 0.81 and 0.14, respectively (critical value 1.61). For equilibrium (b) there is no modelling uncertainty, but (a) has a contribution (labelled ζ) from use of the model ratios ζ_{py} and ζ_{alm}. The strong correlation between them produces a narrow P–T ellipse. The small size of the ζ uncertainty shows that equilibrium geothermobarometry using a reconstructed mineral can be almost as precise as that using only directly measured compositions. Other ellipses in Fig. 7 are like those for non-equilibrium (Fig. 6); the addition of non-equilibrium effects does not noticeably disturb the pattern from other sources.

As garnet is widely used in GTBs, some general remarks on its uncertainties may be helpful, which can be expressed in terms of end-member chemical potentials μ_{gr}, μ_{py} and μ_{alm}. So unsure are the W-block uncertainties that detailed variance–covariance results are not worth presenting. However, derivatives $\partial \mu_i/\partial W_{\alpha\beta}$ depend on composition only [see Appendix C of Supplementary Material, Eq. (C2)] and are relatively reliable. Garnet (b) has a quite ordinary, almandine-rich composition, for which Table 6 shows $\partial \mu_i/\partial W_{\alpha\beta}$. Mukhopadhyay *et al.* (1997) found that uncertainties in the grossular-almandine binary (W_{CaFe} and W_{FeCa}) are much larger than in the other two binary joins (Holdaway, 2000, Fig. 1). Clearly from Table 6, this affects grossular more than the other end-members. Thus, in the current state of knowledge, $\sigma_{\mu,W}$ of grossular must be several times as large as for pyrope or almandine. In geothermometry or geobarometry using a single GTB, grossular does not usually enter into temperature estimation (which relies mainly on Fe–Mg exchange), but is important in P-determining reactions

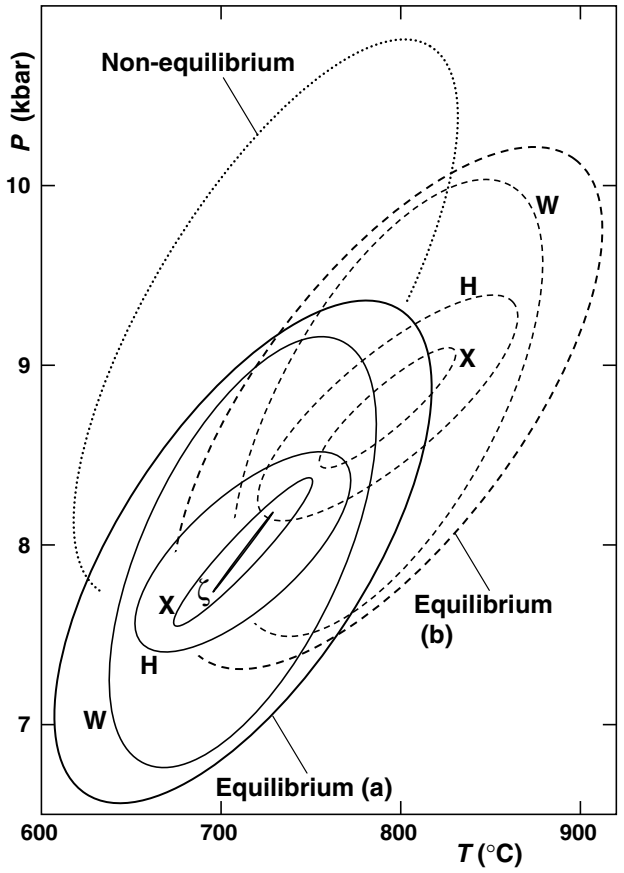

Fig. 7. *P–T* diagram showing uncertainty ellipses (2σ) for hypothetical equilibria in the Yenisey example, using garnet compositions (a) and (b). The overall non-equilibrium ellipse from Fig. 6 is reproduced for comparison.

Table 6. Calculated quantities for garnet (b) in the Yenisey example.

$\partial\mu_i/\partial W_{\alpha\beta}$	i = gr	py	alm
$\alpha\beta$=			
CaMg	0.055	0.113	−0.023
MgCa	0.105	0.069	−0.025
CaFe	0.203	−0.108	0.110
FeCa	0.231	−0.021	−0.010
MgFe	−0.100	0.224	0.099
FeMg	−0.017	0.223	−0.009
CaMgFe (ternary term)	−0.063	−0.076	0.060
Partial derivatives of P_{opt} and T_{opt} in the hypothetical (b) equilibrium:			
$\partial P_{opt}/\partial\mu_i$, kbar (kJ/mol)$^{-1}$	0.081	0.299	0.061
$\partial T_{opt}/\partial\mu_i$,°C (kJ/mol)$^{-1}$	3.3	13.4	−14.3

with plagioclase (in Table 1, reactions 1 and 2). Thus, the grossular uncertainty would be expected to affect pressure rather than temperature. However, this 'grossular effect' is reduced by correlations among μ_i. Also, optimisation tends to nullify the effect, by giving opposite signs of weighting to the two grossular-containing reactions: both $\partial P_{opt}/\partial\mu_{gr}$ and $\partial T_{opt}/\partial\mu_{gr}$ are small (Table 6). This leaves pyrope, the second most uncertain end-member, dominating the uncertainties. Both $\partial P_{opt}/\partial\mu_{py}$ and $\partial T_{opt}/\partial\mu_{py}$ are positive, unsurprisingly as the pyrope content of garnet tends to increase with both P and T. The resulting positive correlation between P_{opt} and T_{opt} is dominant for the W block as a whole (as in Table 4), giving a rather large ellipse elongated in a direction of positive dP/dT (Fig. 7). The effect of the great Ca–Fe uncertainties is somewhat cryptic, though certainly still present; experimentally zeroing them reduces the overall *P–T* uncertainties substantially (and eliminates negative weightings).

In the composition of garnet, the covariances because of constant sum reduce uncertainty. Omitting them in equilibrium (b) increases $\sigma_{P_{opt},XGrt}$ and $\sigma_{T_{opt},XGrt}$ by factors of approximately 1.5 and 1.2, respectively. These are small contributions to overall uncertainties, but covariances should be included to avoid overestimating the X effects.

Departure from equilibrium

Although the uncertainty region for the non-equilibrium *P–T* of reaction greatly overlaps those for hypothetical equilibrium (Fig. 7), statistically significant departure from equilibrium can be demonstrated. Worley & Powell (2000) presented a method of estimating the difference, in equilibrium *P–T*, between two rocks with similar mineral assemblages from different localities. The similarity implies small differences between Jacobians, so that the *P–T* difference is more precisely defined than absolute *P–T*. For present purposes, the difference is between non-equilibrium and equilibrium:

$$\mathbf{J}_{P_{diff}} = \mathbf{J}_{P_{opt},non-eqm} - \mathbf{J}_{P_{opt},eqm},$$

and analogously for temperature. Figure 8 shows results for both equilibria (a) and (b). In case (a), the T difference is small and its uncertainty is very small. This reflects the large part played in non-equilibrium temperature estimation by equilibrium garnet–pyroxene geothermometry using garnet (a), which is explicit in the set of GTBs used (containing both 3a and 4a). In the less special case (b), uncertainties in P and T difference are less than those in absolute *P–T* by roughly a factor of 3.

A garnet composition intermediate between (a) and (b) would give an intermediate result in Figs 7 and 8. The bulk garnet composition is not related to equilibrium at the *P–T* of reaction. The *P–T* band in Fig. 8 corresponds approximately to an uncertainty band for ΔG, of the overall corona-growth reaction producing non-equilibrium garnet, which was estimated non-statistically by Ashworth *et al.* (1998, Fig. 9). The present method does not determine the direction of travel across the *P–T* diagram leading to reaction. If the path is envisaged as vertical (pure P overstep), Fig. 8 shows that the estimated amount is 1.2 ± 0.7 kbar. This supersedes the result, 1.4 ± 0.4 kbar, obtained by Ashworth *et al.* (1998) from rough consideration of only one kind of uncertainty (discrepancies among garnet activity models).

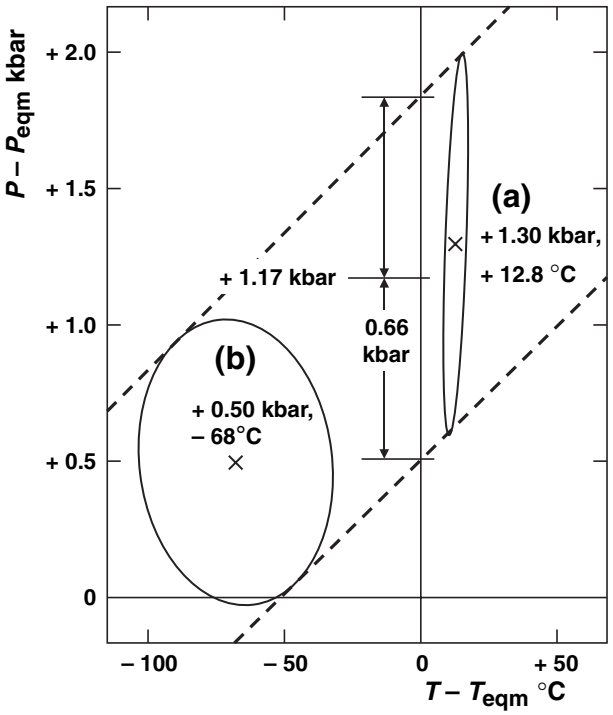

Fig. 8. Overall uncertainty ellipses (2σ) for the differences in P and T between actual non-equilibrium conditions during reaction and the two hypothetical equilibria (a) and (b). The dashed band, tangential to the ellipses, is drawn by eye. Its intersection with the line for $T–T_{eqm} = 0$ is shown as giving an estimate of P overstep if this (at steady T) provided the sole driving force for reaction.

CONCLUSIONS

The statistical method of optimised geothermobarometry has been successfully extended to the non-equilibrium case, incorporating uncertainties from diffusion modelling. These additional uncertainties need not be large, if the reaction texture studied has detailed features providing good petrographic constraints on the modelling. In the example studied, precision is almost as good as in conventional equilibrium geothermobarometry, though subject to an analogous basic approximation (assumed local equilibrium at fixed P–T). Some approximations in the modelling may be improved by future work. For example, if diffusion experiments can provide likely ranges of cross-coefficients, these could be incorporated (instead of neglecting cross-coefficients) in the sampling scheme of inputs to diffusion modelling.

Covariances among diffusion-modelling results affect the outcome. For activity models (often the largest source of uncertainty), covariances may be important in future, and knowledge of them is likely to improve overall precision. In the example, orthopyroxene and plagioclase, near the middles of their solid–solution series, contribute relatively little uncertainty. Garnet, asymmetric in both composition and activity–composition relations, remains problematic.

The reaction studied is sufficiently close to equilibrium for hypothetical equilibrium P and T to be meaningful. This enables departure from equilibrium to be estimated, on a proper statistical basis, in the region of 1 kbar or 100 °C.

ACKNOWLEDGEMENTS

This work was supported by INTAS (97-0325). Dr K. Thomson helped with the computer drawings. The paper was greatly improved following reviews by R. Powell, C. de Capitani and an anonymous referee.

Supplementary Material

The following material is available from: http://www.blackwellpublishing.com/products/journals/suppmat/JMG/JMG552/JMG552sm.htm **Appendix C.** Partial derivatives. Derivation of formulae for use with Eq. (B4). **Appendix D.** Basic programs. Seven Basic modules containing programs and subroutines used in this study.

REFERENCES

Ashworth, J. R. & Birdi, J. J., 1990. Diffusion modelling of coronas around olivine in an open system. *Geochimica et Cosmochimica Acta*, **54,** 2389–2401.

Ashworth, J. R. & Sheplev, V. S., 1997. Diffusion modelling of metamorphic layered coronas with stability criterion and consideration of affinity. *Geochimica et Cosmochimica Acta*, **61,** 3671–3689.

Ashworth, J. R., Sheplev, V. S., Bryxina, N. A., Kolobov, V. Yu. & Reverdatto, V. V., 1998. Diffusion-controlled corona reaction and overstepping of equilibrium in a garnet granulite, Yenisey Ridge, Siberia. *Journal of Metamorphic Geology*, **16,** 231–246.

Ashworth, J. R., Sheplev, V. S., Khlestov, V. V. & Ananyev, V. A., 2001. Geothermobarometry using minerals at non-equilibrium: a corona example. *European Journal of Mineralogy*, **13,** 1153–1161.

Berman, R. G., 1988. Internally consistent thermodynamic data for minerals in the system Na_2O–K_2O–CaO–MgO–FeO–Fe_2O_3–Al_2O_3–SiO_2–TiO_2–H_2O–CO_2. *Journal of Petrology*, **29,** 445–522.

Berman, R. G. & Aranovich, L. Ya., 1996. Optimized standard state and solution properties of minerals I. Model calibration for olivine, orthopyroxene, cordierite, garnet, and ilmenite in the system FeO–MgO–CaO–Al_2O_3–TiO_2–SiO_2. *Contributions to Mineralogy and Petrology*, **126,** 1–24.

Chayes, F., 1971. *Ratio Correlation*. University of Chicago Press, Chicago, IL, USA.

Cheng, W. & Ganguly, J., 1994. Some aspects of multicomponent excess free energy models with subregular binaries. *Geochimica et Cosmochimica Acta*, **58,** 3763–3767.

Davis, J. C., 2002. *Statistics and Data Analysis in Geology*, 3 edn. Wiley, New York, NY, USA.

Fletcher, P., 1993. *Chemical Thermodynamics for Earth Scientists*. Longman, Harlow.

Foster, C. T., 1981. A thermodynamic model of mineral segregations in the lower sillimanite zone near Rangeley, Maine. *American Mineralogist*, **66,** 260–277.

Ganguly, J., Cheng, W. & Tirone, M., 1996. Thermodynamics of aluminosilicate garnet solid solution: new experimental data, an optimized model, and thermometric applications. *Contributions to Mineralogy and Petrology*, **126,** 137–151.

Gordon, T. M., 1992. Generalized thermobarometry: solution of the inverse chemical equilibrium problem using data for individual species. *Geochimica et Cosmochimica Acta*, **56,** 1793–1800.
Helffrich, G. & Wood, B. J., 1989. Subregular model for multicomponent solutions. *American Mineralogist*, **74,** 1016–1022.
Hodges, K. V. & McKenna, L. W., 1987. Realistic propagation of uncertainties in geologic thermobarometry. *American Mineralogist*, **72,** 671–680.
Holdaway, M. J., 2000. Application of new experimental and garnet Margules data to the garnet–biotite geothermometer. *American Mineralogist*, **85,** 881–892.
Holland, T. J. B. & Powell, R., 1985. An internally consistent thermodynamic dataset with uncertainties and correlations: 2. Data and results. *Journal of Metamorphic Geology*, **3,** 343–370.
Holland, T. & Powell, R., 1992. Plagioclase feldspars: activity–composition relations based upon Darken's quadratic formalism and Landau theory. *American Mineralogist*, **77,** 53–61.
Holland, T. & Powell, R., 1996. Thermodynamics of order-disorder in minerals: II. Symmetric formalism applied to solid solutions. *American Mineralogist*, **81,** 1425–1437.
Holland, T. J. B. & Powell, R., 1998. An internally consistent thermodynamic data set for phases of petrological interest. *Journal of Metamorphic Geology*, **16,** 309–343.
Jackson, S. L., 1989. Extension of Wohl's ternary asymmetric solution model to four and *n* components. *American Mineralogist*, **74,** 14–17.
Kohn, M. J. & Spear, F. S., 1991. Error propagation for barometers: 2. Application to rocks. *American Mineralogist*, **76,** 138–147.
Markl, G., Foster, C. T. & Bucher, K., 1998. Diffusion-controlled olivine corona textures in granitic rocks from Lofoten, Norway: calculation of Onsager diffusion coefficients, thermodynamic modelling and petrological implications. *Journal of Metamorphic Geology*, **16,** 607–623.
Milke, R., Wiedenbeck, M. & Heinrich, W., 2001. Grain boundary diffusion of Si, Mg, and O in enstatite reaction rims: a SIMS study using isotopically doped reactants. *Contributions to Mineralogy and Petrology*, **142,** 15–26.
Mukhopadhyay, B., Basu, S. & Holdaway, M.J., 1993. A discussion of Margules-type formulations for multicomponent solutions with a generalized approach. *Geochimica et Cosmochimica Acta*, **57,** 277–283.
Mukhopadhyay, B., Holdaway, M.J. & Koziol, A.M., 1997. A statistical model of thermodynamic mixing properties of Ca–Mg–Fe^{2+} garnets. *American Mineralogist*, **82,** 165–181.
Perkins, D. & Vielzeuf, D., 1992. Experimental investigation of Fe–Mg distribution between olivine and clinopyroxene: implications for mixing properties of Fe–Mg in clinopyroxene and garnet–clinopyroxene thermometry. *American Mineralogist*, **77,** 774–783.
Powell, R., 1978. *Equilibrium Thermodynamics in Petrology*. Harper & Row, London, UK.
Powell, R., 1985. Geothermometry and geobarometry: a discussion. *Journal of the Geological Society, London*, **142,** 29–38.
Powell, R. & Holland, T. J. B., 1985. An internally consistent thermodynamic dataset with uncertainties and correlations: 1. Methods and a worked example. *Journal of Metamorphic Geology*, **3,** 327–342.
Powell, R. & Holland, T. J. B., 1988. An internally consistent dataset with uncertainties and correlations: 3. Applications to geobarometry, worked examples and a computer program. *Journal of Metamorphic Geology*, **6,** 173–204.
Powell, R. & Holland, T., 1993. On the formulation of simple mixing models for complex phases. *American Mineralogist*, **78,** 1174–1180.
Powell, R. & Holland, T., 1994. Optimal geothermometry and geobarometry. *American Mineralogist*, **79,** 120–133.
Powell, R. & Holland, T., 1999. Relating formulations of the thermodynamics of mineral solid solutions: Activity modeling of pyroxenes, amphiboles and micas. *American Mineralogist*, **84,** 1–14.
Powell, R., Holland, T. & Worley, B., 1998. Calculating phase diagrams involving solid solutions via non-linear equations, with examples using THERMOCALC. *Journal of Metamorphic Geology*, **16,** 577–588.
Spear, F. S., 1993. *Metamorphic Phase Equilibria and Pressure–Temperature–Time Paths*. Mineralogical Society of America Monograph, Washington, DC, USA.
Thompson, J. B., 1967. Thermodynamic properties of simple solutions. In: *Researches in Geochemistry* vol. 2 (ed. Abelson, P. H.), pp. 340–361. Wiley, New York, NY, USA.
Wohl, K., 1946. Thermodynamic evaluation of binary and ternary liquid systems. *Transactions of the American Institute of Chemical Engineers*, **42,** 215–249.
Wohl, K., 1953. Thermodynamic evaluation of binary and ternary liquid systems. *Chemical Engineering Progress*, **49,** 218–219.
Worley, B. & Powell, R., 2000. High-precision relative thermobarometry: theory and a worked example. *Journal of Metamorphic Geology*, **18,** 91–101.

Received 6 September 2003; revision accepted 13 October 2004.

APPENDIX A: SIMPLE MATRIX REPRESENTATION OF ACTIVITY MODELS

Most activity models lead directly to Γ_i, defined by

$$\Gamma_i = \mathrm{RT} \ln \gamma_i$$

where γ_i is the activity coefficient of end-member *i*. Then Γ_i is readily used in the expression for chemical potential,

$$\mu_i = \mu_i^0 + \mathrm{RT} \ln x_i + \Gamma_i. \quad \text{(A1)}$$

The expression for Γ_i is usually an elaborate summation, but this appendix shows that it can be computed more simply by matrix formulation.

Multicomponent subregular solid solution

The asymmetric model based on Wohl [1946, Eq. (53)], modified by Wohl, 1953), is used for garnet. Let matrix **W** contain the Margules parameters W_{ij}, including diagonal elements $W_{ii} = 0$. Asymmetry means $W_{ji} \neq W_{ij}$. Using the fact that mole fractions sum to 1, in the absence of ternary (W_{ijk}) or higher parameters, the equation for the excess free energy of mixing, G^{ex} [e.g. Helffrich & Wood, 1989, Eq. (5′)] can be written as the sum of two parts:

$$G^{\mathrm{ex}} = G^{\mathrm{A}} + G^{\mathrm{B}}$$

where

$$G^{\mathrm{A}} = \frac{1}{4}\sum_i \sum_j x_i x_j (W_{ij} + W_{ji}), \quad G^{\mathrm{B}} = \frac{1}{2}\sum_i \sum_j x_i x_j^2 (W_{ij} - W_{ji}). \quad \text{(A2)}$$

This suggests expressing **W** as the sum of symmetric and asymmetric matrices, **A** and **B**:

$$\mathbf{A} = \frac{1}{2}(\mathbf{W} + \mathbf{W}^{\mathrm{T}}) = \mathbf{A}^{\mathrm{T}}, \quad \mathbf{B} = \frac{1}{2}(\mathbf{W} - \mathbf{W}^{\mathrm{T}}) = -\mathbf{B}^{\mathrm{T}},$$

so that, in matrix form,

$$G^{\mathrm{A}} = \frac{1}{2}\mathbf{x}^{\mathrm{T}}\mathbf{A}\mathbf{x}, \quad G^{\mathrm{B}} = \mathbf{x}^{\mathrm{T}}\mathbf{F}\mathbf{x}, \quad \text{(A3)}$$

where column vector **x** contains the mole fractions x_i, and element F_{ij} of **F** is $x_j B_{ij}$.

To find Γ_m for end-member m (Fletcher, 1993, p. 150),

$$\Gamma_m = \left[G^{ex} - \sum_j x_j\left(\frac{\partial G^{ex}}{\partial x_j}\right)\right] + \left(\frac{\partial G^{ex}}{\partial x_m}\right), \tag{A4}$$

in which differentiation treats the x_j as independent variables. The part in square brackets is the same for all m. Differentiating Eq. (A2):

$$\frac{\partial G^A}{\partial x_m} = \frac{1}{4}\left[\sum_i x_i(W_{im} + W_{mi}) + \sum_j x_j(W_{mj} + W_{jm})\right] = \sum_j x_j A_{mj}, \tag{A5a}$$

$$\frac{\partial G^B}{\partial x_m} = \frac{1}{2}\left[\sum_i 2x_i x_m(W_{im} - W_{mi}) + \sum_j x_j^2(W_{mj} - W_{jm})\right] = \sum_j x_j(2F_{jm} + F_{mj}). \tag{A5b}$$

Using matrix representation:

$$\frac{\partial G^{ex}}{\partial x_m} = \frac{\partial(G^A + G^B)}{\partial x_m} = (\mathbf{A}_m + 2\mathbf{F}_m^T + \mathbf{F}_m)\mathbf{x} \tag{A6}$$

where $\mathbf{A}_m$ and $\mathbf{F}_m$ denote the mth row of $\mathbf{A}$ and $\mathbf{F}$. As $\mathbf{x}^T\mathbf{F}^T\mathbf{x} = \mathbf{x}^T\mathbf{F}\mathbf{x}$, the summation over all j in Eq. (A4) is

$$\sum x_j\left(\frac{\partial G^{ex}}{\partial x_j}\right) = \mathbf{x}^T(\mathbf{A} + 3\mathbf{F})\mathbf{x}.$$

Comparing with Eq. (A3), the constant term in Eq. (A4) is

$$G^{ex} - \sum x_j\left(\frac{\partial G^{ex}}{\partial x_j}\right) = -(G^A + 2G^B).$$

Therefore

$$\Gamma_m = \frac{\partial(G^A + G^B)}{\partial x_m} - (G^A + 2G^B). \tag{A7}$$

Using Eq. (A6) and defining

$$\mathbf{D} = \mathbf{A} + \mathbf{F} + 2\mathbf{F}^T,$$

a column vector Γ of all Γ_m is

$$\mathbf{\Gamma} = \mathbf{D}\mathbf{x} - \mathbf{1}(G^A + 2G^B), \tag{A8}$$

in which the effect of pre-multiplying by **1** (a column vector of ones) is that the scalar ($G^A + 2G^B$) is subtracted from every element of the vector. Equation (A8) is equivalent (neglecting ternary interactions) to Eq. (6′) of Helffrich & Wood (1989), Eq. (7) of Jackson (1989), Eq. (22) of Mukhopadhyay *et al.* (1993), and Eq. (5) of Cheng & Ganguly (1994), but is easier to implement by computer programming. The method can be extended to include ternary parameters W_{ijk}. For garnet, Mukhopadhyay *et al.* (1997) used just one of these, W_{123}. The effect in the ternary system is to add to Γ_m

$$x_j x_k(2x_m - 1)W_{123}, \quad k \neq j \neq m.$$

Multi-site models

With mixing on more than one crystallographic site, quantity x_i in Eq. (A1) involves a product of site occupancies (Powell, 1978, Chapter 4). These quantities are not mole fractions (do not generally sum to 1), but can be called ideal activities (e.g. Holland & Powell, 1996). To handle the non-ideal term Γ_i, Powell & Holland (1993) introduced proportions p_i which do sum to 1. A multi-site activity model is then like a single-site one, but with **p** in place of **x**. The models developed by Powell & Holland (1993, 1999) are symmetrical ($W_{ji} = W_{ij}$, and no W_{ijk}). The basic equations in matrix form are those of the last section, simplified by symmetry ($\mathbf{A} = \mathbf{W}$, $\mathbf{B} = \mathbf{F} = \mathbf{0}$) and with **p** instead of **x**. Equation (21) of Powell & Holland (1993) can be written

$$G^{ex} = \frac{1}{2}\mathbf{p}^T\mathbf{W}\mathbf{p}.$$

Unless the end-members used in writing reactions differ from those in the activity model (introducing p^0 of Powell & Holland, 1993), the matrix equation for Γ is Eq. (A8) with symmetrical reduction and **p** instead of **x**:

$$\mathbf{\Gamma} = \mathbf{W}\mathbf{p} - \mathbf{1}G^{ex}.$$

Pure Mg–Fe orthopyroxene is a ternary system because of ordering over two Mg, Fe sites (Holland & Powell, 1996). Ca–Mg–Fe clinopyroxene is approximately binary (see Appendix C of Supplementary Material) and symmetrical (Perkins & Vielzeuf, 1992). For plagioclase, model 3 of Holland & Powell (1992) is used.

APPENDIX B: METHOD OF ESTIMATING UNCERTAINTIES IN P_{OPT} AND T_{OPT}

Jacobians

This section derives the Jacobian (partial-derivative) vectors $\mathbf{J}_{P_{opt}}$ and $\mathbf{J}_{T_{opt}}$, which are split into parts for H, W, X and Q to find the uncertainty ellipses in the main text. Following Powell & Holland (1988, Appendix C), to find the weightings of GTBs, $\mathbf{w}_P$ in P_{ave} and $\mathbf{w}_T$ in T_{ave}, requires full Jacobian matrices $\mathbf{J}_P$ and $\mathbf{J}_T$ containing $\partial P_{esti}/\partial y_j$ and $\partial T_{esti}/\partial y_j$ for all GTBs i. Then

$$\mathbf{J}_{P_{ave}} = \mathbf{w}_P\mathbf{J}_P, \quad \mathbf{J}_{T_{ave}} = \mathbf{w}_T\mathbf{J}_T. \tag{B1}$$

From the geometry of intersecting lines (Fig. B1),

$$\frac{\partial P_{opt}}{\partial y} = \frac{\partial P_{ave}}{\partial y} + \frac{\partial P_{ave}}{\partial T}\frac{\partial T_{opt}}{\partial y},$$
$$\frac{\partial T_{opt}}{\partial y} = \frac{\partial T_{ave}}{\partial y} + \frac{\partial T_{ave}}{\partial P}\frac{\partial P_{opt}}{\partial y}.$$

Rearranging and writing full vectors **J**,

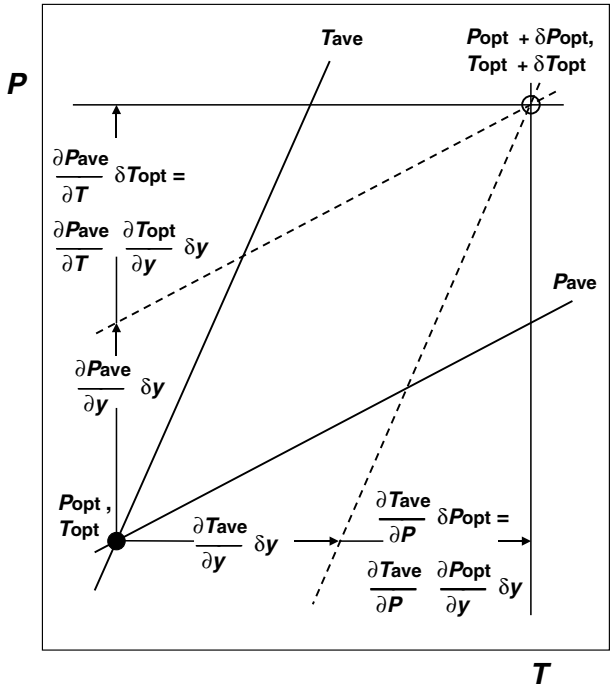

Fig. B1. Geometrical effect of an increment δy in one of the quantities y used in geothermobarometry. The intersection of the lines for P_{ave} and T_{ave} is displaced from P_{opt}, T_{opt} to $P_{opt} + \delta P_{opt}$, $T_{opt} + \delta T_{opt}$.

$$\left[1-\left(\frac{\partial P_{\rm ave}}{\partial T}\right)\left(\frac{\partial T_{\rm ave}}{\partial P}\right)\right]\mathbf{J}_{P_{\rm opt}}=\mathbf{J}_{P_{\rm ave}}+\left(\frac{\partial P_{\rm ave}}{\partial T}\right)\mathbf{J}_{T_{\rm ave}}, \qquad \text{(B2a)}$$

$$\left[1-\left(\frac{\partial P_{\rm ave}}{\partial T}\right)\left(\frac{\partial T_{\rm ave}}{\partial P}\right)\right]\mathbf{J}_{T_{\rm opt}}=\mathbf{J}_{T_{\rm ave}}+\left(\frac{\partial T_{\rm ave}}{\partial P}\right)\mathbf{J}_{P_{\rm ave}}. \qquad \text{(B2b)}$$

Being derived from the same set of GTBs, $\mathbf{J}_{P_{\rm ave}}$, $\mathbf{J}_{T_{\rm ave}}$, $\partial P_{\rm ave}/\partial T$ and $\partial T_{\rm ave}/\partial P$ are closely related. Useful for checking numerical accuracy is that ρ, found from $\sigma_{P_{\rm opt}}$, $\sigma_{T_{\rm opt}}$ and Cov($P_{\rm opt}$, $T_{\rm opt}$), should satisfy the following equality (evident in Fig. 6 of Powell & Holland, 1994):

$$\rho^2=\left(\frac{\partial P_{\rm ave}}{\partial T}\right)\left(\frac{\partial T_{\rm ave}}{\partial P}\right). \qquad \text{(B3)}$$

Central approximation

Non-equilibrium casts doubt on the validity of linear error propagation, i.e. treating all partial derivatives as constants. In general, if $\partial P_{\rm est}/\partial y$ and $\partial T_{\rm est}/\partial y$ are measured at the same P–T point, their relationship (underlying those exemplified by Eq. (B3)) is

$$s\left(\frac{\partial T_{\rm est}}{\partial y}\right)=-v\left(\frac{\partial P_{\rm est}}{\partial y}\right)=\frac{\partial g}{\partial y} \qquad \text{(B4)}$$

where

$$g=\Delta G_{\rm A}-Q\Delta G_{\rm B},\quad s=\Delta S_{\rm A}-Q\Delta S_{\rm B},\quad v=\Delta V_{\rm A}-Q\Delta V_{\rm B}.$$

The disturbing aspect of non-equilibrium is the presence of derivatives with respect to Q, which clearly vary with P and T because

$$\frac{\partial g}{\partial Q}=-\Delta G_{\rm B}. \qquad \text{(B5)}$$

Therefore, in this study, rather than linearising before finding $P_{\rm opt}$, $T_{\rm opt}$ (Worley & Powell, 2000), derivatives are obtained at $P_{\rm opt}$, $T_{\rm opt}$ and at other P–T points as a check on approximate linearity. The result at $P_{\rm opt}$, $T_{\rm opt}$, used in drawing the ellipses, is called the central approximation. It is achieved iteratively. Preliminary estimates of $P_{\rm opt}$ and $T_{\rm opt}$ are used to refine $P_{\rm opt}$, then this refinement is used in refining $T_{\rm opt}$, and so on. At the beginning of each step, derivatives are evaluated at current estimated $P_{\rm opt}$, $T_{\rm opt}$. After convergence, these give unchanged $P_{\rm opt}$ or $T_{\rm opt}$ at the end of the step. Because GTB lines do not pass through the P–T point in use, $\partial P_{\rm est}/\partial y$ and $\partial T_{\rm est}/\partial y$ cannot be measured directly but are defined in terms of $\partial g/\partial y$, s and v by Eq. (B4). Quantities s and v are themselves partial derivatives, and are calculated as such:

$$s=-\frac{\partial g}{\partial T},\quad v=\frac{\partial g}{\partial P}.$$

For the linearity check, in the example, nominal uncertainties were computed at $P_{\rm opt}\pm 2\rho\sigma_{P_{\rm opt}}$, $T_{\rm opt}\pm 2\rho\sigma_{T_{\rm opt}}$ (Table B1). Overall values are satisfactorily within a few percent of those at $P_{\rm opt}$, $T_{\rm opt}$ (Table 4). As expected, non-linearity is most evident in the Q uncertainties, but these remain small.

The simplest way to estimate most derivatives is by finite differences [Worley & Powell, 2000, Eq. (12)]. However, the analytical interpretation in this paper refers to exact formulae for some. Finding them is made easier by the matrix formulation of activity models (Appendix A), as shown in Appendix C of Supplementary Material. The programs (see Appendix D of Supplementary Material) use a full set of formulae.

Near-degeneracy and near-equivalence

This section explains the limitations on how many non-equilibrium GTBs are used. The set must not be degenerate, i.e. the algebraic formula for one g must not be a linear combination of the others. Two sets of mineral compositions (a) and (b) have vectors of end-member chemical potentials $\boldsymbol{\mu}_{\rm a}$ and $\boldsymbol{\mu}_{\rm b}$. The vector $\mathbf{g}$ of g_i for GTBs i is

$$\mathbf{g}=\mathbf{R}_{\rm a}\boldsymbol{\mu}_{\rm a}+\mathbf{R}_{\rm b}\boldsymbol{\mu}_{\rm b}$$

where the $\mathbf{R}$ matrices combine stoichiometric coefficients and Q ratios. For example, for the set of GTBs 2a/1a, 1b/1a, 2b/1a:

Table B1. Nominal uncertainties at $P_{\rm opt}-2\rho\sigma_{P\rm opt}$, $T_{\rm opt}-2\rho\sigma_{T\rm opt}$ and $P_{\rm opt}+2\rho\sigma_{P\rm opt}$, $T_{\rm opt}+2\rho\sigma_{T\rm opt}$ for the Yenisey non-equilibrium example.

	P–T					
	8.13 kbar, 649 °C			10.38 kbar, 801 °C		
	$\sigma_{P\rm opt,\lambda}$ (kbar)	$\sigma_{T\rm opt,\lambda}$ (°C)	ρ_λ	$\sigma_{P\rm opt,\lambda}$ (kbar)	$\sigma_{T\rm opt,\lambda}$	ρ_λ
Nominal λ=						
H	0.302	30.1	0.811	0.344	31.6	0.824
W	0.641	37.9	0.741	0.673	37.9	0.771
X	0.142	17.1	0.558	0.182	20.7	0.627
Q	0.162	4.5	−0.145	0.248	11.7	0.685
	$\sigma_{P\rm opt}$	$\sigma_{T\rm opt}$	ρ	$\sigma_{P\rm opt}$	$\sigma_{T\rm opt}$	ρ
Nominal overall	0.740	51.6	0.698	0.817	54.8	0.738

$$\mathbf{R}_{\rm a}=\begin{bmatrix}\boldsymbol{\nu}_2 & - & Q_{\rm 2a/1a} & \boldsymbol{\nu}_1\\ & - & Q_{\rm 1b/1a} & \boldsymbol{\nu}_1\\ & - & Q_{\rm 2b/1a} & \boldsymbol{\nu}_1\end{bmatrix},\quad \mathbf{R}_{\rm b}=\begin{bmatrix}\mathbf{0}\\ \boldsymbol{\nu}_1\\ \boldsymbol{\nu}_2\end{bmatrix}, \qquad \text{(B6)}$$

where $\boldsymbol{\nu}_i$ is the row vector of stoichiometric coefficients for reaction i. Vector $\mathbf{g}$ would be degenerate if one ratio was a combination of the others (e.g. 2b/1b, 1b/1a, 2b/1a), provided that mutually consistent Q values are used. This limits the number of GTBs thus:

$$n_{\rm GTB}\le n_{\rm set}\cdot n_{\rm reac}-1,$$

where $n_{\rm set}$ is the number of sets of mineral compositions (a, b, c, …), and $n_{\rm reac}$ is the number of independent reactions (four in the example).

Degeneracy affects optimisation through the partial derivatives, because matrices $\mathbf{V}_P(=\mathbf{J}_P\mathbf{V}\mathbf{J}_P^{\rm T})$ and analogous $\mathbf{V}_T$ are inverted to find weightings. Except for the Q block [Eq. (B5)],

$$\frac{\partial\mathbf{g}}{\partial y}=\mathbf{R}_{\rm a}\left(\frac{\partial\boldsymbol{\mu}_{\rm a}}{\partial y}\right)+\mathbf{R}_{\rm b}\left(\frac{\partial\boldsymbol{\mu}_{\rm b}}{\partial y}\right)\quad(y\ne Q_i).$$

If $\mathbf{g}$ is degenerate, non-Q parts of $\mathbf{J}_P$ and $\mathbf{J}_T$ are degenerate. Then if Q uncertainties are small, $\mathbf{V}_P$ and $\mathbf{V}_T$ are nearly singular, and weightings cannot be reliably defined. Now, if composition sets (a) and (b) are similar, $\partial\boldsymbol{\mu}_{\rm a}/\partial y$ and $\partial\boldsymbol{\mu}_{\rm b}/\partial y$ will be very similar or identical for many y. In the example, (a) and (b) differ only (and slightly) in garnet composition. Therefore the non-Q parts of $\mathbf{J}_P$ and $\mathbf{J}_T$ are nearly degenerate if the combined matrix $\mathbf{R}_{\rm a}+\mathbf{R}_{\rm b}$ is degenerate, i.e. there exists a row vector $\mathbf{a}$ such that

$$\mathbf{a}(\mathbf{R}_{\rm a}+\mathbf{R}_{\rm b})=\mathbf{0}.$$

That degeneracy is present in Eq. (B6), with

$$a_1=1-Q_{\rm 1b/1a},\quad a_2=Q_{\rm 2a/1a}-Q_{\rm 2b/1a},\quad a_3=Q_{\rm 1b/1a}-1.$$

In the Yenisey example, Q uncertainties are small enough that this type of near-degeneracy makes matrix inversion unreliable. It occurs if any subset of n' GTBs uses fewer than n' reactions. Avoiding it restricts the number of GTBs (with $n_{\rm set}>1$) to

$$n_{\rm GTB}=n_{\rm reac},$$

hence $n_{\rm GTB}=4$ in the Yenisey example. This is the same number as in equilibrium geothermobarometry using the same end-members. In a sense, the equilibrium GTBs remain in use, but are modified to account for non-equilibrium. Evidently, two mineral composition sets give more information than one, but little would be gained by introducing a third, intermediate set of mineral compositions.

A second kind of near-degeneracy is associated with strong correlations among Q ratios. First considering the Q block in isolation, a perfect correlation in $\mathbf{V}_Q$ would make $\mathbf{V}_{P,Q}$ and $\mathbf{V}_{T,Q}$ singular; strong correlations can induce near-singularity. In the example, $\mathbf{V}_{P,Q}$ and $\mathbf{V}_{T,Q}$ are in fact exactly singular, because the two equilibrium GTBs have Q-block uncertainties solely from ζ and degenerate. If, to avoid this, an equilibrium GTB is replaced by a non-equilibrium one, the

strong Q correlations make the matrix inversion unstable; weightings could still not be properly defined using the Q block alone. Now, these correlations imply approximate relationships among the model analogues of ΔG, exemplified by Eq. (7). If these were exact, and if chemical potentials in the geothermobarometry perfectly matched the pattern predicted by the modelling, then $\mathbf{V}_P$ and $\mathbf{V}_T$ as a whole would be singular. In the real example, inversion tends to be unstable if more than two non-equilibrium GTBs are used. Using two ratios from the strongly correlated set conveys sufficient information.

Because near-degeneracies are inexact, different sets of four GTBs are not exactly, but nearly equivalent. The chosen set is one of at least ten that give P_{opt}, T_{opt},$\sigma_{P_{\mathrm{opt}}}$ and $\sigma_{T_{\mathrm{opt}}}$ within ranges of $\pm 1\%$. Singular Value Decomposition of a matrix, advocated by Powell & Holland (1985) in another context, should indicate how many GTBs to retain in a less simple case, with more disparate mineral compositions or more freedom in the modelling.